

RESEARCH ARTICLE

Characterization of a Novel Model of Lumbar Ligamentum Flavum Hypertrophy in Bipedal Standing Mice

Zhen-yu Zheng, MD^{1†}, Peng Li, MD^{1†} , Xiang Ao, MD¹, Lei Qian, MD², Yong-xing Peng, MD¹, Jun Chu, MD¹, Tao Jiang, MD¹, Zheng-nan Lian, MD¹, Zhong-min Zhang, MD^{1,3}, Liang Wang, MD¹

¹Department of Orthopaedics, The Third Affiliated Hospital, Southern Medical University, Academy of Orthopaedics and ²Department of Anatomy, Guangdong Province Key Laboratory of Medical Biomechanics and ³Division of Spine Surgery, Department of Orthopaedics, Nanfang Hospital, Southern Medical University, Guangzhou, China

Objective: To explore the main causes of hypertrophied ligamentum flavum (HLF) and the possibility of using bipedal standing mouse model to simulate the pathological changes in human HLF.

Methods: Thirty-two 8-week-old C57BL/6 male mice were randomly assigned to the experimental group ($n = 16$) and control group ($n = 16$). In the experimental group, mice were induced to adopt a bipedal standing posture by their hydrophobia. The experimental mice were maintained bipedal standing for 8 h a day with an interval of 2 h to consume food and water. The control mice were placed in a similar environment without bipedal standing. Eight 18-month-old C57BL/6 male mice were compared to evaluate the LF degeneration due to aging factor. Three-dimensional (3D) reconstruction and finite element models were carried out to analyze the stress and strain distribution of the mouse LF in sprawling and bipedal standing postures. Hematoxylin and Eosin (HE), Verhoeff-Van Gieson (VVG), and immunohistochemistry (IHC) staining were used to evaluate the LF degeneration of mice and humans. RT-qPCR and immunofluorescence analysis were used to evaluate the expressions of fibrosis-related factors and inflammatory cytokines of COL1A1, COL3A1, α -SMA, MMP2, IL-1 β , and COX-2.

Results: The von Mises stress (8.85×10^{-2} MPa) and maximum principal strain (6.64×10^{-1}) in LF were increased 4944 and 7703 times, respectively, in bipedal standing mice. HE staining showed that the mouse LF area was greater in the bipedal standing 10-week-old group ($[10.01 \pm 2.93] \times 10^4 \mu\text{m}^2$) than that in the control group ($[3.76 \pm 1.87] \times 10^4 \mu\text{m}^2$) and 18-month-old aged group ($[6.09 \pm 2.70] \times 10^4 \mu\text{m}^2$). VVG staining showed that the HLF of mice (3.23 ± 0.58) and humans (2.23 ± 0.31) had a similar loss of elastic fibers and an increase in collagen fibers. The cell density was higher during the process of HLF in mice (39.63 ± 4.81) and humans (23.25 ± 2.05). IHC staining showed that the number of α -SMA positive cells were significantly increased in HLF of mice (1.63 ± 0.74) and humans (3.50 ± 1.85). The expressions of inflammatory cytokines and fibrosis-related factors of COL1A1, COL3A1, α -SMA, MMP2, IL-1 β , and COX-2 were consistently higher in bipedal standing group than the control group.

Conclusion: Our study suggests that 3D finite element models can help analyze the abnormal stress and strain distributions of LF in modeling mice. Mechanical stress is the main cause of hypertrophied ligamentum flavum compared to aging. The bipedal standing mice model can reflect the pathological characteristics of human HLF. The bipedal standing mice model can provide a standardized condition to elucidate the molecular mechanisms of mechanical stress-induced HLF *in vivo*.

Key words: Aging; Finite element analysis; Hypertrophy of ligamentum flavum; Mechanical stress; Mouse model

Address for correspondence Zhong-min Zhang, MD, Division of Spine Surgery, Department of Orthopaedics, Nanfang Hospital, Southern Medical University, Guangzhou, China 510515; Tel and Fax: 020-62787195; Email: nfzsm@163.com; Liang Wang, MD, Department of Orthopaedics, The Third Affiliated Hospital, Southern Medical University, Academy of Orthopaedics, Guangzhou, China 510630; Tel and Fax: 020-62784300; Email: liang091@aliyun.com

[†]Zhen-yu Zheng and Peng Li contributed equally to this work as co-first authors.

Disclosure: The authors declare that they have no competing interests.

Received 19 January 2021; accepted 15 September 2021

Introduction

Lumbar spinal stenosis (LSS) is one of the most common spinal diseases and has a high incidence among the increasingly elderly population¹. Various factors including disc protrusion, facet osteoarthritis, and hypertrophied ligamentum flavum (HLF) were reported to lead to the development of LSS. Of note, HLF is considered as one of the major causes of LSS²⁻⁴. Usually, ligamentum flavum (LF) is a protective spinal ligament covering the posterior wall of the spinal canal. Histologically, normal LF is an elastic ligament tissue that consists of 20% collagen fibers and 80% elastic fibers. In contrast, hypertrophied LF showed increased collagen fibers, loss of elastic fibers, calcification, ossification, and chondrometaplasia, suggesting degenerative changes^{2,3,5}. LF occupies a large space of the lateral and posterior of the spinal canal, which is susceptible to LF morphological and pathological changes. A degenerative and thickening of LF can cause lumbar spinal stenosis and compresses the nerve roots or cauda equina, thereby leading to low back pain and intermittent claudication⁵. Presently, the only therapeutic method for LSS patients caused by HLF is operation. An understanding of the physiopathological mechanism of HLF would be valuable. A variety of factors including age, activity level, genetic composition, and mechanical stress accelerate the development of HLF⁶. At present, there are two main causes of HLF: aging and mechanical stress⁶⁻¹⁵. However, which factor plays a decisive role in HLF remains unknown. It has been suggested that an abnormal mechanical stress can accelerate the degradation and hypertrophy of LF due to the micro-injuries to the LF tissue^{11,13,14}. Repeated micro-injuries lead to chronic inflammation and subsequent tissue scarring, which eventually cause HLF^{9,10}. An *in vitro* study has demonstrated that mechanical tension promotes collagen synthesis *via* the TGF- β 1 pathway⁷. Overall, further understanding the key role of mechanical stress in the development of HLF will shed light on its prevention and treatment.

Although many studies have revealed its underlying molecular mechanisms *in vitro*, the effects of abnormal stress on HLF have not been fully studied *in vivo* due to a lack of animal models. Mice are common and cost-efficient animal models for medical research. The use of mice models to study the effects of mechanical loading has received increasing attention in recent years, partly because of the advantages of such models in terms of cost, access to specimens, and controllable load level. However, only one complicated stretch device has been used to model HLF in mice¹⁶. After 12 weeks of consecutive flexion-extension loading on mice spine, Saito *et al.*¹⁶ found a significant increase of collagen area in the mouse LF. Several limitations associated with this HLF model are shown for its complicated operation, requirement for repeated anesthesia, and mild LF pathological changes. Hayashi *et al.*¹⁷ established a rabbit HLF model in which intervertebral mechanical stress was concentrated on LF with adjacent segment fusion operations. These animal models may not represent the HLF degeneration process in

humans. As these models are established using quadrupedal animals, the lumbar spinal kinematics may be different from bipedal humans. Therefore, it is necessary to create a bipedal animal model that replicates the LF degeneration in humans.

Based on a previous study of spinal degeneration¹⁸, our study used bipedal standing mice to make HLF. With the increased application of finite element analysis in medicine, the analysis of abnormal stress on HLF has gradually become available. Finite element analysis was used to verify the hypothesis that mouse LF is hypertrophied under abnormal tension. Employing finite element model can be helpful to obtain the mechanical parameters that are difficult to capture by traditional biomechanical method. Micro-CT combined with finite element research can help to intuitively analyze the mechanical problems at the microscopic level and enable the biomechanical analysis of the mouse LF.

In previous studies, only human samples harvested during spine surgery were used to investigate the degeneration of the LF. However, disease severity, disease duration, and other factors will affect the research results¹⁷. For example, Sairyo *et al.*¹⁰ found that the inflammation-related enzyme cyclooxygenase 2 (COX2) and interleukin-1 β (IL-1 β) were similarly expressed in both thin and thick ligaments, and they considered that inflammatory cytokines may appear before hypertrophy occurs, since inflammation could be the initial stage of hypertrophy. Consequently, it is necessary to build a standard condition in an animal model to elucidate the molecular mechanisms of LF hypertrophy.

The aims of this study were: (i) to analyze the stress changes of LF in bipedal standing mice by FEA analysis; (ii) to compare the effects of aging and mechanical stress of HLF by mice modeling; and (iii) to identify the possibility of simulating the pathological changes of human HLF with bipedal standing mice.

Materials and Methods

Animals and Experimental Procedure

All animal experiments were approved by the Animal Experimental Ethics Committee of the Southern Medical University. To eliminate the possible effects of estrogen, a total of 32 eight-week-old C57BL/6 male mice were randomly assigned to the control group ($n = 16$) and experimental (bipedal standing) group ($n = 16$). In the experimental group, the hydrophobia of mice was used to induce a bipedal posture as previously described¹⁸. The mice were placed in a cylindrical chamber with 5 mm of water at the bottom to induce the bipedal standing posture. The mice were maintained in a bipedal standing posture for 6 h a day with an interval of 2 h of free activity to consume food and water. The control mice were placed in a similar environment without water at the bottom. Eight mice from each group were randomly selected and euthanized at 6 or 10 weeks to assess the degree of LF degeneration. Since no significant difference was found in LF degeneration between the 14-week-old and 18-week-old mice in the control group, the 18-week-old mice

were taken as the control group. To study the effect of aging on the degeneration of LF, additional eight 18-month-old C57BL/6 male mice were randomly selected as older mice to evaluate the LF degeneration due to aging.

Three-Dimensional (3D) Reconstruction of Finite Element Model

The mice were anesthetized and subjected to a micro-CT scan (LaTheta LCT-100S; Aloka, Tokyo, Japan). The anesthetized mice were secured in the scanning capsule in the sprawling and bipedal standing postures. The scanning parameters were as follows: 55 kV, 109 μ A, slice thickness 96 μ m, exposure time 200 ms, and pixels 512 \times 512. A total of 650 and 606 images of the L₅-L₆ segment were obtained in DICOM data format with the mice in the sprawling and bipedal standing positions, respectively. The image data were imported into Mimics 14.0 (Materialize Corp., Leuven, Belgium) for 3D reconstruction of L₅-L₆ segment. The reconstructed STL files were imported into Hypermesh 13.0 (Altair, Troy, MI, USA) for meshing. Then, the data were introduced to Abaqus 6.14 (Dassault Systemes Simulia Corp., Providence, RI, USA) for material property assignment. The endplate was a shell unit, and the ligament (except the LF) and joint capsule were spring units. The LF was a truss unit, and the other components were tetrahedral units. The friction coefficient of the joint was 0.1¹⁹. The material properties of each component are shown in Table 1. To analyze the mechanical stress on the LF, a single force of 0.2 N (half the body weight of the mouse) was applied to the vertebral body to calculate the degree and distribution of the stress and strain on the LF.

TABLE 1 Composition and material properties of each component

Components	Material and Property	Cited Reference
Annulus ground substance	Hyper elastic Mooney-Rivlin C01 = C10 = 0.1; C02 = C11 = C20 = 0.01; D1 = D2 = 35	Hsieh <i>et al.</i> ²⁰
Nucleus pulposus	Hyper elastic Mooney-Rivlin C01 = 0.01; C10 = 0; D1 = 100	Hsieh <i>et al.</i> ²⁰
Endplate	Elastic, E = 100, ν = 0.2	Argoubi <i>et al.</i> ²¹
Cancellous bone	Elastic, E = 50, ν = 0.2	Silva <i>et al.</i> ²²
Cortical bone	Elastic, E = 148000, ν = 0.3	Lambers <i>et al.</i> ²³
LF	Hyper elastic Mooney-Rivlin E = 15 (<6.2%), 19.5 (>6.2%) 0.3	Chen <i>et al.</i> ²⁴

Finite Element Analysis of Mouse Ligamentum Flavum

Von Mises Stress

Von Mises stress is practically an equivalent stress and is generally used to show the stress distributions in the model, clearly showing the results of stress changes in the entire model²⁵.

Maximum Principal Strain

Maximum principal strain, which is actually a maximal strain on a certain part of a model, is usually used to represent the maximum strain distribution in a model and can clearly represent the result of maximum stress change in one direction.

Human LF Sample Collection

The Ethics Committee of the Third Affiliated Hospital of Southern Medical University approved the experiment, and each patient provided informed consent before surgery. During surgery, specimens were obtained from eight patients diagnosed with LSS and HLF and eight patients with lumbar disc herniation but without HLF. The dorsal layer of LF tissues were taken from the same anatomical region (L_{4/5}). The age and gender distributions are shown in Table S1.

Histological Analysis

After euthanasia, the intact L₅ and L₆ lumbar vertebrae of mice were obtained and fixed in neutral formaldehyde, decalcified, dehydrated, embedded in paraffin, and sectioned to a thickness of 4 μ m. Human LF were treated without decalcification, and other treatments were the same as those of the mice. To visualize the area of LF, elastic fibers, and collagen fibers within the LF, Hematoxylin and Eosin (H&E) staining (C0105, Beyotime, China) and Verhoeff-Van Gieson (VVG) staining (DC0059, Leagene, China) were performed according to the manufacturer's instructions. Each specimen was measured three times, and the average value was taken.

Area of Mouse LF

Mouse LF area was measured in H&E staining specimen and calculated by ImageJ (National Institutes of Health, USA) software.

Ratio of Elastic Fibers to Collagen Fibers

The ratio of elastic fibers to collagen fibers of mouse/human LF was measured in VVG staining specimen and calculated by ImageJ software.

Cell Density

The cell density of mouse/human LF was measured in H&E staining specimen and calculated by Image J software.

Immunohistochemistry and Immunofluorescence Analysis

The sections were deparaffinized, hydrated and incubated in citrate buffer with heating for 16 h at 60°C. Sections for

immunohistochemistry were treated with 3% H₂O₂ for 10 min to quench the endogenous peroxidase activity. The sections were washed three times for 5 min in phosphate-buffered saline (PBS) and blocked in 5% goat serum at room temperature for 1 h. The sections were stained with the primary antibody anti- α -smooth muscle actin (α -SMA) (1:100, A11111, ABclonal) for immunohistochemistry. The sections were incubated with primary antibodies against COL1A1 (1:100, ab254113, Abcam), COL3A1 (1:100, AF5457, Affinity), α -SMA (1:100, A11111, ABclonal), MMP2 (1:100, ab92536, Abcam), IL-1 β (1:100, A16288, ABclonal), and COX-2 (1:100, ab179800, Abcam) for immunofluorescence. Species-matched secondary antibody was used. Then, DAB (DAB-0031, MXB-Bio, China) was used for immunohistochemistry, and DAPI (ab104139, Abcam) was used for immunofluorescence.

Positive Cells of COL1A1, COL3A1, α -SMA, MMP2, IL-1 β and COX-2

The positive cells of COL1A1, COL3A1, α -SMA, MMP2, IL-1 β and COX-2 of mouse/human LF were measured in immunohistochemistry and immunofluorescence specimens and calculated by Image J software.

Image Quantification

LF Thickness in MRI

The thickness of the human LF was measured at the facet joint of the L_{4/5} level with axial T1-weighted magnetic resonance imaging (MRI) (Philips, Amsterdam, The Netherlands) as described in our previous study²⁶.

Histological Images

The histological images were obtained using a digital light microscope (Axio Scope. A1, Zeiss, Germany). All quantitative data was counted by investigators who were blinded to the group assignments.

RT-qPCR Analysis

Another 32 eight-week-old C57BL/6 male mice were randomly assigned to the control group ($n = 16$) and experimental group ($n = 16$). Mice from each group were euthanized at 10 weeks and the LF were obtained with the aid of an operating microscope (Olympus SZX 16, Japan). Human LF specimens were obtained from 8 HLF patients and 8 non-HLF patients. RNeasy Micro Kit (74004, Qiagen, Germany) was used to extract total RNA from LF cells. HiScript II Q SuperMix (R323-01, Vazyme, China) was used

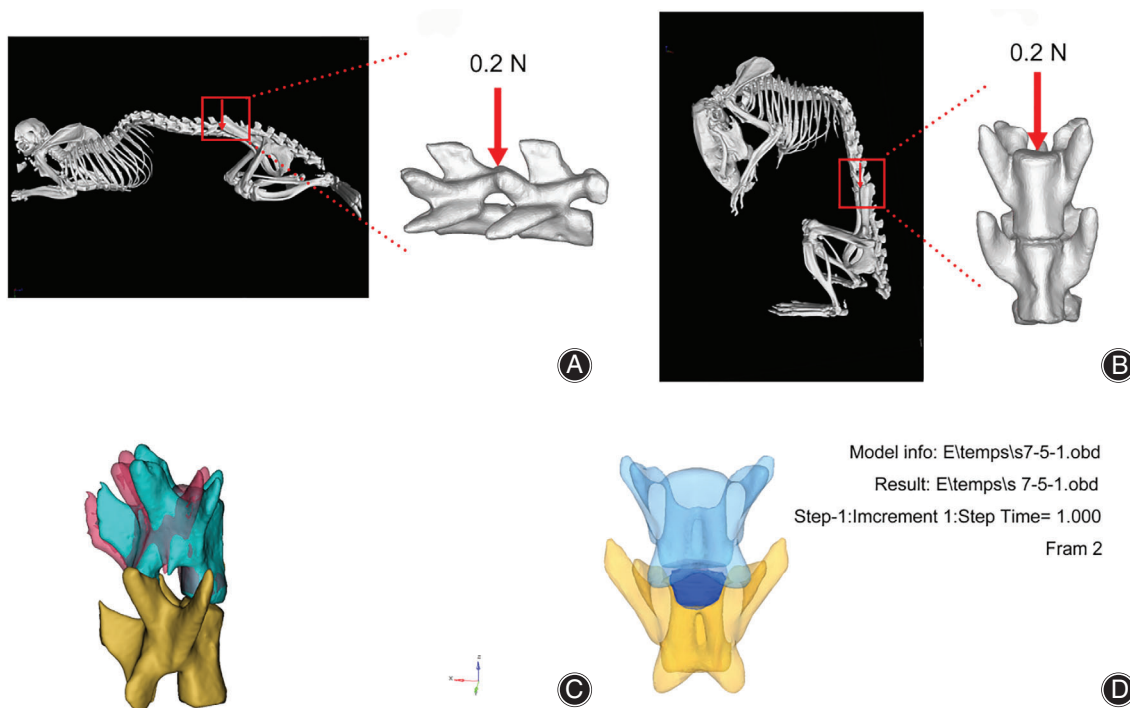


Fig. 1 Simulation of different stress states in mice lumbar models. 3D simulation mouse model in the (A) sprawling posture and (B) bipedal standing posture. (C) The relative position of the L₅ in the sprawling and bipedal standing postures. The pink vertebrae represents the L₅ position in the sprawling posture, and the light blue vertebrae represents the L₅ position in the bipedal standing posture. (D) The dark blue area represents the anatomical location of the LF.

for the reverse transcription reaction. The qPCR reaction was performed with ChamQ SYBR qPCR Master Mix (Q311-02, Vazyme, China). The primers were synthesized by Sangon Biotech (Shanghai, China). Mouse and human primers used are listed in Tables S2 and S3. β -actin was used as an internal reference. The data were analyzed using the $2^{-\Delta\Delta C_t}$ method²⁷.

Statistical Analysis

All statistical analyses were performed using SPSS 22.0 (SPSS Inc., Chicago, IL, USA). The data were expressed as means \pm SD. Student's *t*-test was used to compare data between the two groups. One-way analysis of variance (ANOVA) was used for comparisons among multiple groups. $P < 0.05$ indicated significant differences.

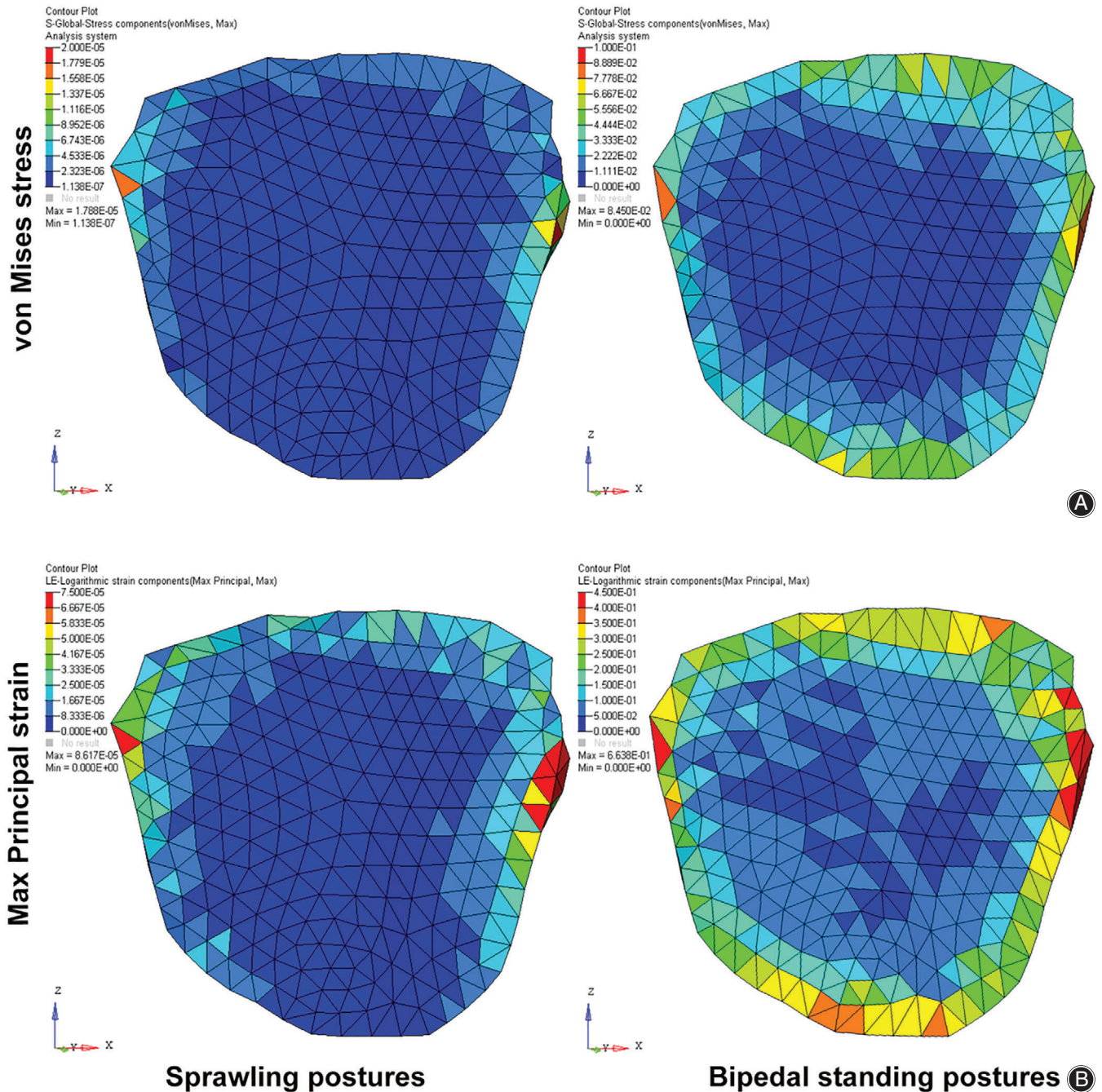


Fig. 2 Changes in posture altered the stress on the mouse LF. (A) The distribution and values of von Mises stress of the LF in the sprawling and bipedal standing postures. (B) The distribution and values of the maximum principal strain of the LF in the sprawling and bipedal standing postures.

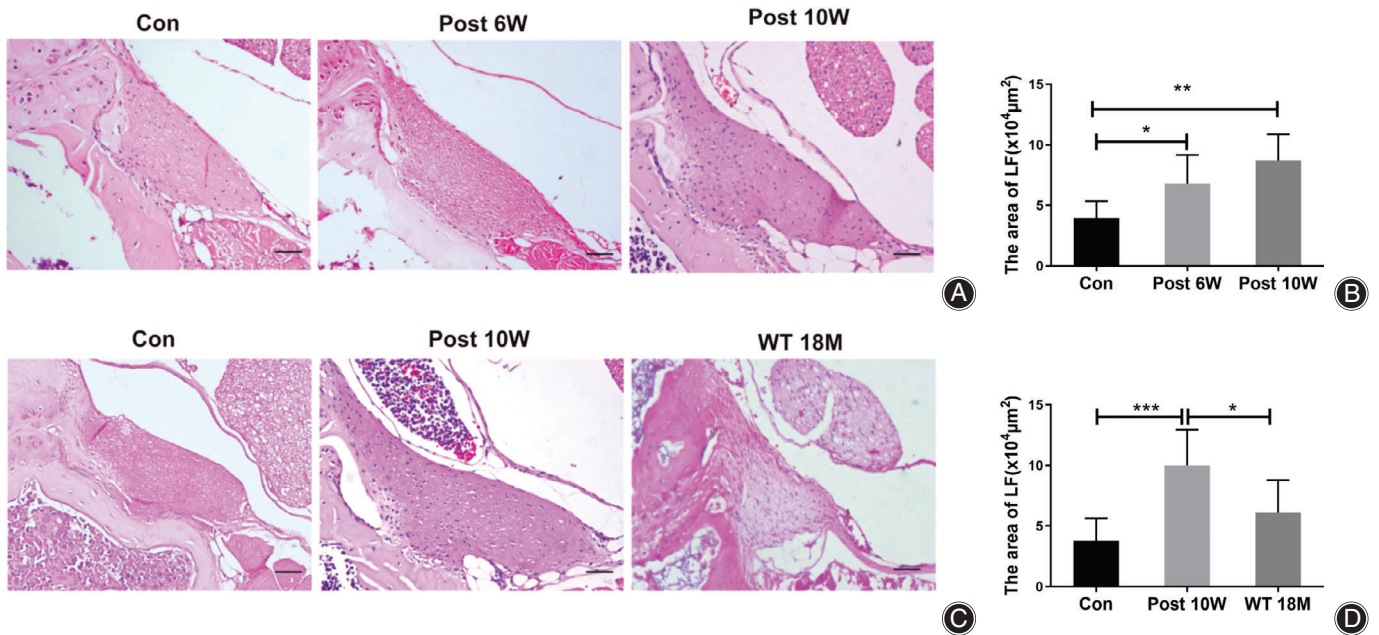


Fig. 3 Mouse LF areas were measured in control, bipedal standing, and old groups. (A) H&E staining of LF specimens from different groups. (B) The statistical results of mice LF area in different groups ($n = 8$). (C) H&E staining of LF specimens from different groups. (D) Statistical results of the mice LF area in different groups ($n = 8$). ANOVA was used. $*P < 0.05$, $***P < 0.001$. Error bars show means \pm SD, scale bars = 20 μm ; Con = control group = 18-week-old non-bipedal standing group; Post 6W = post 6-week bipedal standing group; Post 10W = post 10-week bipedal standing group; WT 18M = wild-type aged mice at 18 months.

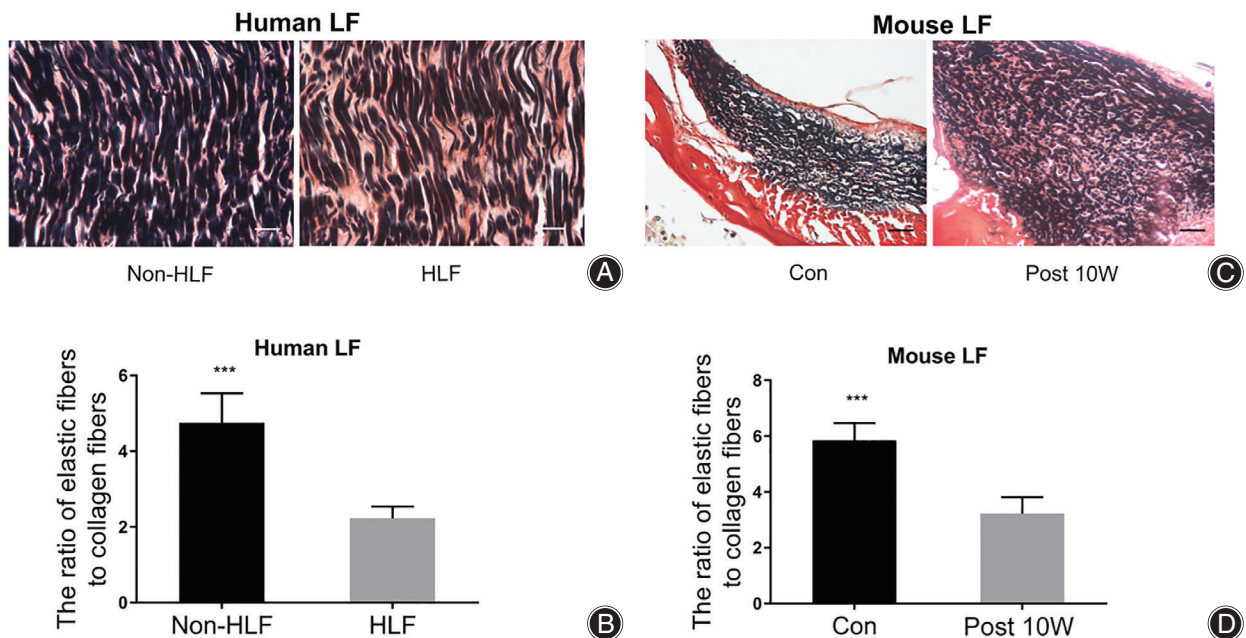


Fig. 4 ECM changed in bipedal standing mouse and human LF. (A) VVG staining of human LF. The elastic fibers were purple-black, the collagen fibers were red. (B) Quantitative analyses of the ratio of elastic fibers to collagen fibers in human LF ($n = 8$). (C) VVG staining of mouse LF. (D) Quantitative analyses of the ratio of elastic fibers to collagen fibers in mouse LF ($n = 8$). Student's t -test was used. $***P < 0.001$. Scale bars = 10 μm . Error bars show means \pm SD.

Results

Von Mises Stress and Maximum Principal Strain

The 3D mice models were constructed to simulate the sprawling and bipedal standing postures (Fig. 1A and Fig. 1B). The L₅ vertebral body flexed anteriorly in reference to the L₆ when the mice were in the bipedal postures (Fig. 1C). The ligamentum flavum lies between the lamina (Fig. 1D). The stress and strain on the LF were primarily concentrated in the LF near the facet joint. In the sprawling posture, the von Mises stress was 1.79×10^{-5} MPa, and the maximum principal strain was 8.62×10^{-5} (Fig. 2A). When the mice were in the bipedal posture, the von Mises stress value increased to 8.85×10^{-2} MPa, and the maximum principal strain increased to 6.64×10^{-1} (Fig. 2B). The von Mises stress and maximum principal strain in LF were increased 4944 and 7703 times, respectively, in bipedal standing mice.

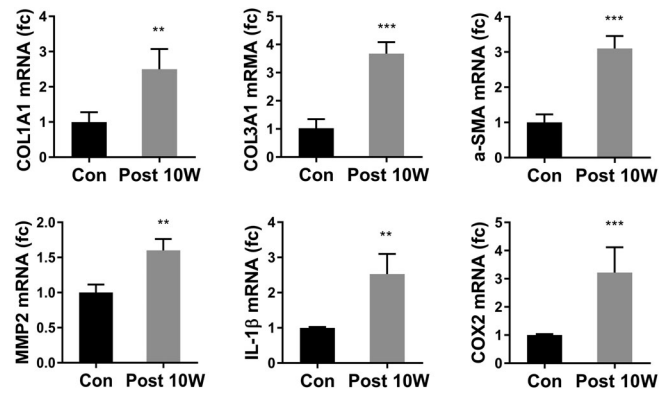


Fig. 6 Increased gene expression of inflammatory cytokines and fibrosis-related factors in the bipedal standing mice. RT-qPCR was used to detect the expression of COL1A1, COL3A1, α-SMA, MMP2, IL-1β and COX-2 in the control and 10-week bipedal standing groups. Student's *t*-test was used. ***P* < 0.01, ****P* < 0.001. Results represent for independent experiments with four mice each. Error bars show means ± SD.

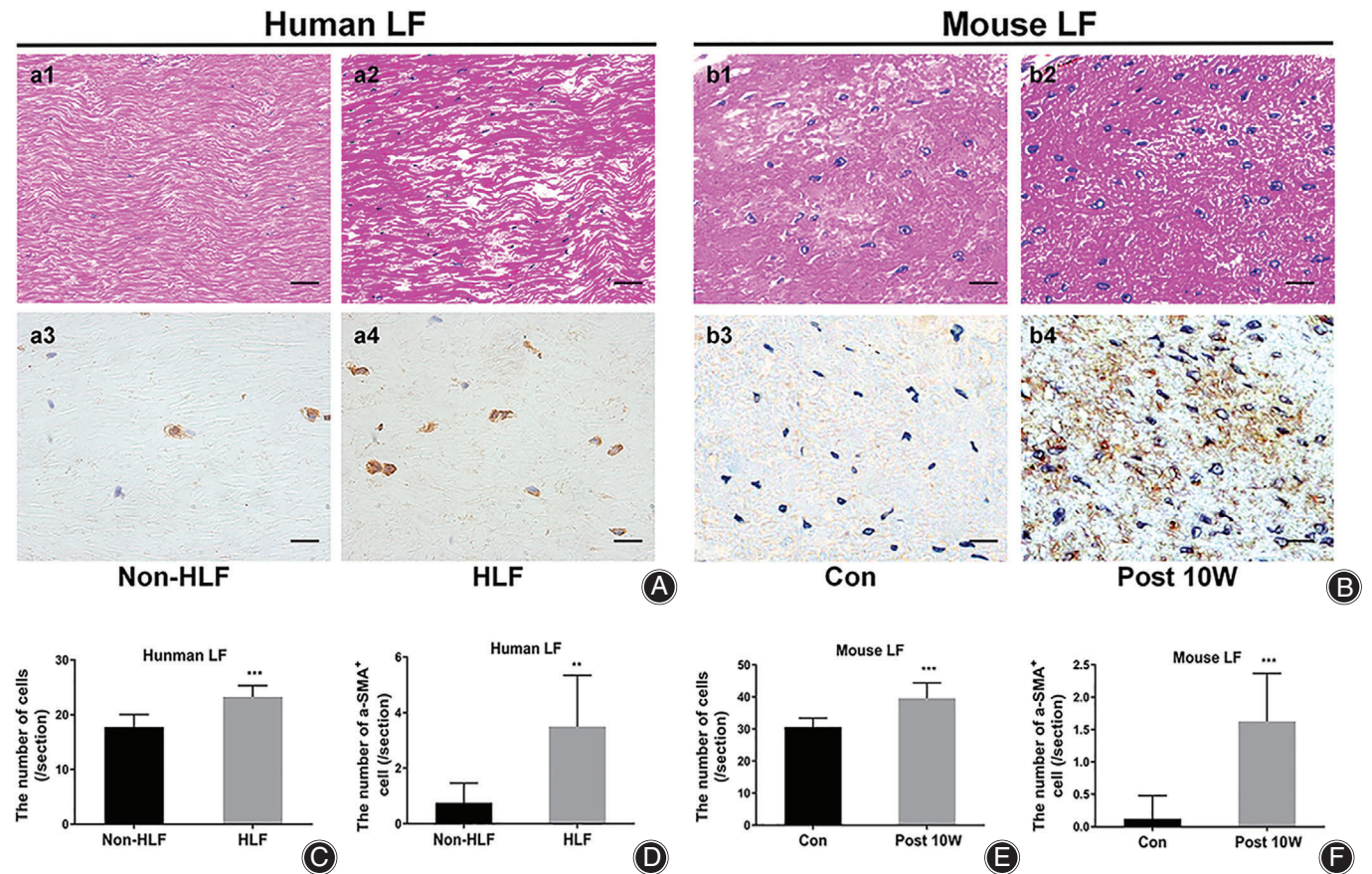


Fig. 5 Changes in the cell density and cell type. (A) In human LF samples, the cell density and the number of α-SMA-positive cells in different groups. (B) In mouse LF samples, the cell density and the number of α-SMA-positive cells in different groups. (C) Quantitative analyses of human LF cell density (*n* = 8). (D) Quantitative analyses of α-SMA-positive cells in human LF (*n* = 8). (E) Quantitative analyses of mice LF cell density (*n* = 8). (F) Quantitative analyses of α-SMA-positive cells in mice LF (*n* = 8). Student's *t*-test was used. ***P* < 0.01, ****P* < 0.001. Scale bars a1, a2 = 50 μm; a3, a4 = 20 μm; B = 5 μm. Error bars show means ± SD.

Mouse LF

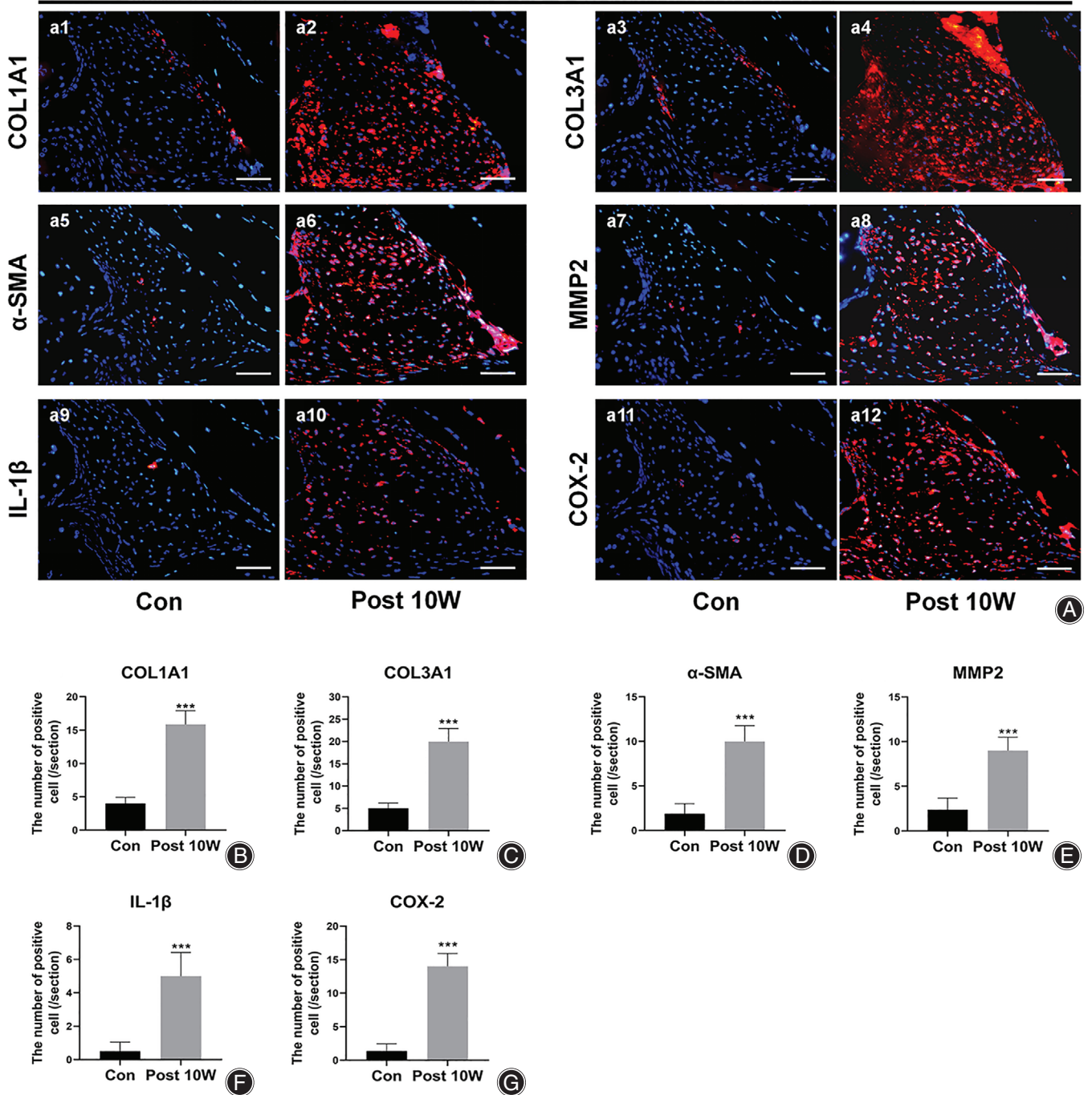


Fig. 7 Increased protein expression of inflammatory cytokines and fibrosis-related factors in the bipedal standing mice. (A) In mice LF sections, immunofluorescence staining was used to detect the expression of COL1A1, COL3A1, α-SMA, MMP2, IL-1β, and COX-2 in the control and 10-week bipedal standing groups. Scale bars = 50 μm. (B-G) Quantitative analyses of positive cells of COL1A1, COL3A1, α-SMA, MMP2, IL-1β, and COX-2 in mice LF ($n = 8$). Student's t -test was used. *** $P < 0.001$. Error bars show means \pm SD.

LF Area Increased in Bipedal Standing Mice

H&E staining showed that the area of the LF in the bipedal standing groups (Post 6W = $[6.78 \pm 2.39] \times 10^4 \mu\text{m}^2$; Post

10W = $[8.71 \pm 2.16] \times 10^4 \mu\text{m}^2$) were larger than that in the control group ($[3.94 \pm 1.40] \times 10^4 \mu\text{m}^2$) (Fig. 3A,B). Furthermore, the area of the LF was larger in the 10-week

bipedal standing group ($[10.01 \pm 2.93] \times 10^4 \mu\text{m}^2$) than that in the control group ($[3.76 \pm 1.87] \times 10^4 \mu\text{m}^2$) and 18-month-old group ($[6.09 \pm 2.70] \times 10^4 \mu\text{m}^2$) (Fig. 3C,D). Although aging can also cause HLF, no significant difference was observed between the 18-month-old group and the control group ($P = 0.06$; Fig. 3D).

LF Pathological Changes

This study presented the extracellular matrix (ECM) changes of LF in bipedal standing mice and humans. VVG staining showed that the HLF patients had a significant loss of elastic fibers and an increase in collagen fibers. In humans, the ratio of elastic fibers to collagen fibers was lower in HLF specimens (2.23 ± 0.31) than in non-HLF specimens (4.75 ± 0.78) (Fig. 4A,B). Similarly, the ratio of elastic fibers to collagen fibers also lower in 10-week bipedal standing mice (3.23 ± 0.58) than control mice (5.85 ± 0.62) (Fig. 4C,D). In addition to changes in the ECM, the number of cells and cell types also changed during the process of HLF in humans and mice. In humans, the cell density was higher in HLF (23.25 ± 2.05) than non-HLF specimens (17.75 ± 2.32) (Fig. 5a1,a2,C). The number of α -SMA-positive cells were higher in HLF (3.50 ± 1.85) than non-HLF specimens (0.75 ± 0.71) (Fig. 5a3,a4,D). Similarly, the cell density in the LF was significantly higher in the bipedal standing mice (39.63 ± 4.81) than control mice (30.63 ± 2.83) (Fig. 5b1,b2,E). The number of α -SMA-positive cells in the LF were higher in the 10-week bipedal standing mice (1.63 ± 0.74) than control mice (0.13 ± 0.35) (Fig. 5b3,b4,F). The HLF pathology in the bipedal standing mice is identical to that in humans.

LF Fibrosis and Inflammatory Cytokines

In mice LF, the relative gene expression levels were evaluated by RT-qPCR assay. COL1A1 (2.50 ± 0.57), COL3A1 (3.68 ± 0.41), α -SMA (3.10 ± 0.36), MMP2 (1.60 ± 0.16), IL-1 β (2.53 ± 0.57), and COX-2 (3.22 ± 0.90) mRNA expression levels were

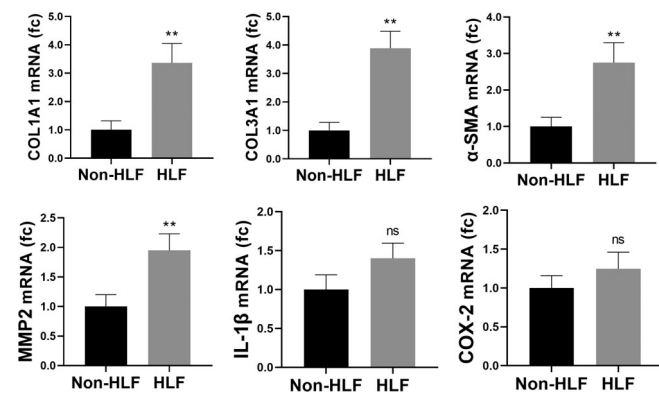


Fig. 8 Increased gene expression of inflammatory cytokines and fibrosis-related factors in the HLF patients. RT-qPCR was used to detect the expression of COL1A1, COL3A1, α -SMA, MMP2, IL-1 β , and COX-2 in non-HLF patients ($n = 8$) and HLF patients ($n = 8$). Student's t -test was used. ** $P < 0.01$, ns, not significant. Error bars show means \pm SD.

over-expressed in the 10-week bipedal standing groups (Fig. 6). The protein expression levels in mice LF were evaluated by immunofluorescence assay. The number of positive cells for COL1A1 (15.88 ± 2.03), COL3A1 (20.13 ± 2.90), α -SMA (10.38 ± 1.85), MMP2 (9.13 ± 1.55), IL-1 β (5.17 ± 1.47), and COX-2 (13.75 ± 2.05) were higher in the 10-week bipedal standing mice than control mice (Fig. 7). In human LF, the relative gene expression levels of COL1A1 (3.36 ± 0.69), COL3A1 (3.89 ± 0.59), α -SMA (2.75 ± 0.55), MMP2 (1.95 ± 0.28), IL-1 β (1.40 ± 0.19), and COX-2 (1.25 ± 0.21) were over-expressed in the HLF patients (Fig. 8). The number of positive cells for COL1A1 (9.83 ± 1.46), COL3A1 (12.17 ± 1.47), α -SMA (7.17 ± 0.75), MMP2 (5.83 ± 1.47), IL-1 β (1.17 ± 1.16), and COX-2 (0.66 ± 0.51) were higher in HLF patients than non-HLF patients (Fig. 9).

Discussion

Mechanical stress and aging might control the metabolism of the LF matrix and the expression of various fibrosis-associated factors by affecting the biological behavior of LF cells²⁸. To investigate the main external factors that cause HLF and establish an animal model of HLF will help in the study of the molecular signal transduction mechanism of LF hypertrophy.

Key Role of Mechanical Stress in Bipedal Mice

Axial sections showed that the lateral part of mice LF originated from the medial part of facet joint and was primarily located in this region, showing an approximate triangular shape. The LF on both sides were connected by membrane like LF. Finite element analysis showed that the anterior tilting of the L₅ in a bipedal standing posture can stretch the LF. The von Mises stress and maximum principal strain on the LF remarkably increased, which exceeded our previous estimates. H&E staining showed a significant increase of LF area in bipedal standing mice compared to the control group. In addition, this study showed that although aging can lead to HLF, there was no significant difference in LF area between the aging group and the control group. Therefore, mechanical stress may be the main cause of HLF. Increased stress and strain in the LF may cause micro-injuries, which induce the production of inflammatory and fibrosis factors and, ultimately, HLF.

Pathological Similarities between Mouse and Human LF

The bipedal standing mouse can simulate the pathological changes of human HLF. A feature of fibrosis is the trans-differentiation of fibroblasts into activated myofibroblasts, which express α -SMA²⁹. In the bipedal standing mice, our study found that the greater number of α -SMA-positive cells, the higher cell density, and the lower ratio of LF elastic fibers to collagen fibers. These changes were identical with the pathological changes in the human HLF (Figs 4,5).

Human LF

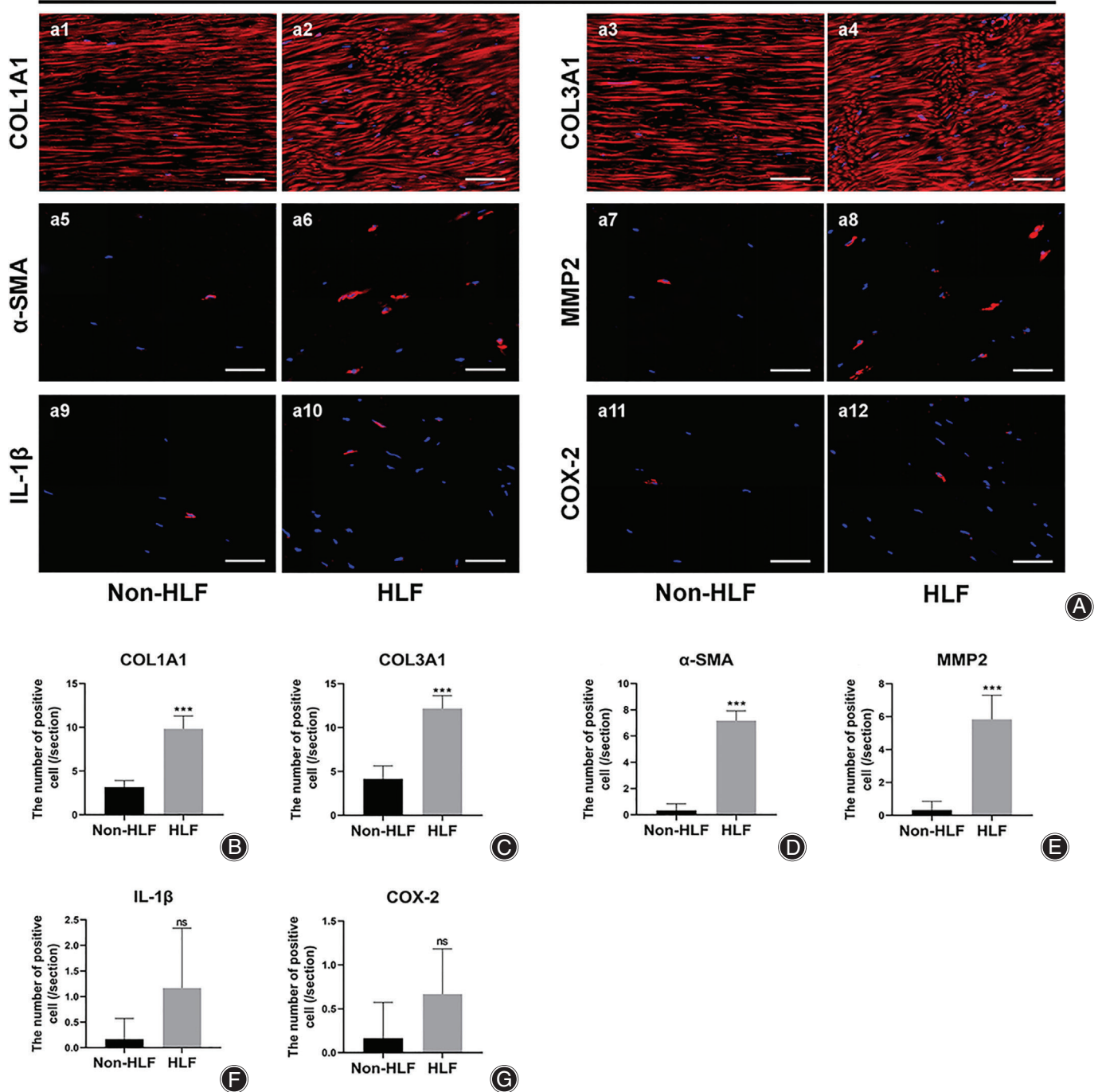


Fig. 9 Increased protein expression of inflammatory cytokines and fibrosis-related factors in the HLF patients. (A) In human LF sections, immunofluorescence staining was used to detect the expression of COL1A1, COL3A1, α -SMA, MMP2, IL-1 β , and COX-2 in the non-HLF and HLF patients. Scale bars = 50 μ m. (B-G) Quantitative analyses of positive cells of COL1A1, COL3A1, α -SMA, MMP2, IL-1 β , and COX-2 in human LF ($n = 8$). Student's t -test was used. *** $P < 0.001$, ns, not significant. Error bars show means \pm SD.

Differences in Current Animal Models of HLF

Bipedal standing mice can imitate the posture of humans when bending forward. CT reconstruction showed that when

the mice were in a bipedal posture, the spine flexed, which is close to the posture of human spine flexion. In contrast to the model developed by Saito *et al.*¹⁶, who studied the effect

of stress on LF using a tension loading device, bipedal standing mice can simulate the change of anatomical position of human spine. In contrast to the rabbit model of lumbar internal fixation, this model can avoid the interference of trauma in the process of spinal degeneration¹⁷. Mouse models can provide more accurate data on the biological reaction of the LF to mechanical stress under standardized conditions. Sairyo *et al.*¹⁰ suggested that expression of inflammatory cytokines may occur prior to hypertrophy in humans. They found that the inflammatory cytokines such as IL-1 β and COX-2 were detected in both thin (control) and thick (hypertrophied) ligamentum flavum and were similarly expressed. However, in the mouse model, IL-1 β and COX-2 expression between the control and bipedal standing groups was different.

Limitations of the Study

Mice cannot be used to develop an LSS model because the ratio of the LF to the dural tube is significantly smaller in mice than in humans. Nevertheless, the bipedal standing mouse can be used to reflect the pathological characteristics of human HLF. The bipedal mouse model can be used in

transgenic mice, and study of specific gene expression in mechanical stress-induced HLF *in vivo* will be realized.

Acknowledgments

This work was supported by National Natural Science Foundation of China (81874013, 81672228 and 81702199).

Ethical Approval

The animal experiments were approved by the Animal Experimental Ethics Committee of the Southern Medical University. The Ethics Committee of the Third Affiliated Hospital of Southern Medical University approved the human experiment.

Supporting Information

Additional Supporting Information may be found in the online version of this article on the publisher's web-site:

Table S1. General data of patients. Independent-sample *t*-test; *P* < 0.05 is considered to be significant. **Table S2** Primers used for qRT-PCR (Mice). **Table S3** Primers used for qRT-PCR (Human).

References

- Szpalski M, Gunzburg R. Lumbar spinal stenosis in the elderly: an overview. *Eur Spine J*, 2003, 12: S170–S175.
- Park JB, Chang H, Lee JK. Quantitative analysis of transforming growth factor-beta 1 in ligamentum flavum of lumbar spinal stenosis and disc herniation. *Spine (Phila Pa 1976)*, 2001, 26: E492–E495.
- Jirathanathornnukul N, Limthongkul W, Yingsakmongkol W, Singhatanadgige W, Parkpian V, Honsawek S. Increased expression of vascular endothelial growth factor is associated with hypertrophic ligamentum flavum in lumbar spinal canal stenosis. *J Invest Med*, 2016, 64: 882–887.
- Sakai Y, Ito S, Hida T, Ito K, Harada A, Watanabe K. Clinical outcome of lumbar spinal stenosis based on new classification according to hypertrophied ligamentum flavum. *J Orthop Sci*, 2017, 22: 27–33.
- Costandi S, Chopko B, Mekhail M, Dews T, Mekhail N. Lumbar spinal stenosis: therapeutic options review. *Pain Pract*, 2015, 15: 68–81.
- Sairyo K, Biyani A, Goel V, *et al.* Pathomechanism of ligamentum flavum hypertrophy: a multidisciplinary investigation based on clinical, biomechanical, histologic, and biologic assessments. *Spine (Phila Pa 1976)*, 2005, 30: 2649–2656.
- Nakatani T, Marui T, Hitora T, Doita M, Nishida K, Kurosaka M. Mechanical stretching force promotes collagen synthesis by cultured cells from human ligamentum flavum via transforming growth factor-beta1. *J Orthop Res*, 2002, 20: 1380–1386.
- Park JB, Lee JK, Park SJ, Riew KD. Hypertrophy of ligamentum flavum in lumbar spinal stenosis associated with increased proteinase inhibitor concentration. *J Bone Joint Surg Am*, 2005, 87: 2750–2757.
- Kosaka H, Sairyo K, Biyani A, *et al.* Pathomechanism of loss of elasticity and hypertrophy of lumbar ligamentum flavum in elderly patients with lumbar spinal canal stenosis. *Spine (Phila Pa 1976)*, 2007, 32: 2805–2811.
- Sairyo K, Biyani A, Goel VK, *et al.* Lumbar ligamentum flavum hypertrophy is due to accumulation of inflammation-related scar tissue. *Spine (Phila Pa 1976)*, 2007, 32: E340–E347.
- Kong MH, Morishita Y, He W, *et al.* Lumbar segmental mobility according to the grade of the disc, the facet joint, the muscle, and the ligament pathology by using kinetic magnetic resonance imaging. *Spine (Phila Pa 1976)*, 2009, 34: 2537–2544.
- Haig AJ, Adewole A, Yamakawa KS, Kelemen B, Aagesen AL. The ligamentum flavum at L4-5: relationship with anthropomorphic factors and clinical findings in older persons with and without spinal disorders. *PM R*, 2012, 4: 23–29.
- Moon HJ, Park YK, Ryu Y, *et al.* The angiogenic capacity from ligamentum flavum subsequent to inflammation: a critical component of the pathomechanism of hypertrophy. *Spine (Phila Pa 1976)*, 2012, 37: E147–E155.
- Shafaq N, Suzuki A, Terai H, Wakitani S, Nakamura H. Cellularity and cartilage matrix increased in hypertrophied ligamentum flavum: histopathological analysis focusing on the mechanical stress and bone morphogenetic protein signaling. *J Spinal Disord Tech*, 2012, 25: 107–115.
- Yoshiiwa T, Miyazaki M, Notani N, Ishihara T, Kawano M, Tsumura H. Analysis of the relationship between ligamentum flavum thickening and lumbar segmental instability, disc degeneration, and facet joint osteoarthritis in lumbar spinal stenosis. *Asian Spine J*, 2016, 10: 1132–1140.
- Saito T, Yokota K, Kobayakawa K, *et al.* Experimental mouse model of lumbar ligamentum flavum hypertrophy. *PLoS One*, 2017, 12: e0169717.
- Hayashi K, Suzuki A, Abdullah Ahmadi S, *et al.* Mechanical stress induces elastic fibre disruption and cartilage matrix increase in ligamentum flavum. *Sci Rep*, 2017, 7: 13092.
- Ao X, Wang L, Shao Y, *et al.* Development and characterization of a novel bipedal standing mouse model of intervertebral disc and facet joint degeneration. *Clin Orthop Relat Res*, 2019, 477: 1492–1504.
- Polikeit A, Ferguson SJ, Nolte LP, Orr TE. Factors influencing stresses in the lumbar spine after the insertion of intervertebral cages: finite element analysis. *Eur Spine J*, 2003, 12: 413–420.
- Hsieh AH, Wagner DR, Cheng LY, Lotz JC. Dependence of mechanical behavior of the murine tail disc on regional material properties: a parametric finite element study. *J Biomech Eng*, 2005, 127: 1158–1167.
- Argoubi M, Shirazi-Adl A. Poroelastic creep response analysis of a lumbar motion segment in compression. *J Biomech*, 1996, 29: 1331–1339.
- Silva MJ, Keaveny TM, Hayes WC. Load sharing between the shell and centrum in the lumbar vertebral body. *Spine (Phila Pa 1976)*, 1997, 22: 140–150.
- Lambers FM, Schulte FA, Kuhn G, Webster DJ, Müller R. Mouse tail vertebrae adapt to cyclic mechanical loading by increasing bone formation rate and decreasing bone resorption rate as shown by time-lapsed *in vivo* imaging of dynamic bone morphometry. *Bone*, 2011, 49: 1340–1350.
- Chen CS, Cheng CK, Liu CL, Lo WH. Stress analysis of the disc adjacent to interbody fusion in lumbar spine. *Med Eng Phys*, 2001, 23: 483–491.
- Peng YX, Zheng ZY, Wang Md WG, *et al.* Relationship between the location of ligamentum flavum hypertrophy and its stress in finite element analysis. *Orthop Surg*, 2020, 12: 974–982.
- Zheng Z, Ao X, Li P, *et al.* CRLF1 is a key regulator in the ligamentum flavum hypertrophy. *Front Cell Dev Biol*, 2020, 8: 858.
- Livak KJ, Schmittgen TD. Analysis of relative gene expression data using real-time quantitative PCR and the 2^{-ΔΔC_T} method. *Methods*, 2001, 25: 402–408.
- Hur JW, Kim BJ, Park JH, *et al.* The mechanism of ligamentum flavum hypertrophy: introducing angiogenesis as a critical link that couples mechanical stress and hypertrophy. *Neurosurgery*, 2015, 77: 274–281 discussion 281–282.
- Wynn TA. Cellular and molecular mechanisms of fibrosis. *J Pathol*, 2008, 214: 199–210.